Journal of the Serbian Chemical Society
JSCS-info@shd.org.rs • www.shd.org.rs/JSCS
J. Serb. Chem. Soc. *75* (9) 1167–1179 (2010)
JSCS–4040
UDC 547.461.5:576.385.5:616–006.04
Original scientific paper

Antiproliferative activity of NCI-DTP glutarimide derivatives. An alignment independent 3D QSAR study

JELENA B. POPOVIĆ-DJORDJEVIĆ[1]*, LJILJANA I. DOŠEN-MIĆOVIĆ[2#], IVAN O. JURANIĆ[2#] and BRANKO J. DRAKULIĆ[3#]

[1]*Faculty of Agriculture, University of Belgrade, Nemanjina 6, 11080 Belgrade,* [2]*Faculty of Chemistry, University of Belgrade, Studentski trg 12–16, 11000 Belgrade and* [3]*ICTM – Department of Chemistry, University of Belgrade, Njegoševa 12, 11000 Belgrade, Serbia*

(Received 2 December 2009, revised 25 January 2010)

Abstract: Alignment-free, three dimensional structure–activity relationships (3D QSAR) of the antiproliferative potency of twenty-two glutarimide-containing compounds, taken from National Cancer Institute Developmental therapeutics Program database, toward eight representative human tumour cell lines are reported. The descriptors used in the QSAR study were derived from GRID molecular interaction fields. The obtained models readily detect structural motifs positively or negatively correlated with the potency of the studied compounds toward each cell line. In this way, the pharmacophoric pattern required for high potency of compounds is reported. This pattern can serve as guidance for the design and syntheses of novel congeners, planned to be tested toward human tumour cell lines.

Keywords: glutarimides; antiproliferative agents; alignment-independent 3D QSAR; GRIND descriptors.

INTRODUCTION

Nitrogen-containing heterocyclic systems having different pharmacological activities are widespread among alkaloids. Five- and six-membered cyclic imide derivatives are a valuable group of bioactive compounds, which act as androgen receptor antagonists, anti-inflammatory agents, anxiolytics, antivirals, antibacterials, and tumour suppressing agents.[1] These compounds rarely occur in natural sources and most of them are made synthetically.

Cancer may affect people at all ages, animals or even plants; it causes about 13 % of all human deaths. Consequently, huge efforts are being made in the search for and exploration of new antitumour agents. In light of the present re-

* Corresponding author. E-mail: jelenadj@agrif.bg.ac.rs
# Serbian Chemical Society member.
doi: 10.2298/JSC091202076P

cession in the world and the reduction of financing in R&D, all pharmaceutical companies retain the development of antitumour agents as top priority projects.

Some naturally occurring glutarimides, such as sesbanimides, cycloheximide, and streptimidone, were investigated as antibiotics during the 60–70s of the last century. Later, it was discovered that they act as very potent cytotoxic agents.[2,3] Recent research in the field of human medicine shows that cycloheximide increases the cytotoxic effect of the recombinant human tumour necrosis factor-α (rHuTNF-α) to nasopharyngeal carcinoma cells (NPC).[4] The structurally related streptimidone derivative, 9-methylstreptimidone (9-MS), exerts significant inhibitory activity to the cancer and inflammatory cells activated nuclear factor-κB (NF-κB).[5]

The non-steroidal aromatase inhibitor aminoglutethimide is used for the treatment of Cushing's syndrome[6] and hormone-sensitive metastatic breast cancer.[7,8] Estrone derivatives with the D-ring replaced with the glutarimide ring have shown potent inhibition of steroid sulphatase, an enzyme which is involved in the pathway of the development of hormone-dependent breast tumours (HDBT).[9] 2-Phenylamino-imidazo[4,5-*h*]isoquinolin-9-ones, inhibitors of kinase p56 (lck) in T-cells, were recently reported as potential therapeutic agents in the treatment of different autoimmune diseases.[10]

The GRIND, alignment independent, interpretable and efficient to compute descriptors derived from GRID molecular interaction fields, was proved relevant in diverse structure–activity relationship studies. The GRIND was used for structure–activity relationships in receptors or enzymes, the classification of large structurally diverse datasets by pharmacophore similarity and virtual screening.[11] Regarding the antiproliferative activity of organic compounds, the structure-based rationalization of the mechanism of action of antitumour drugs on NCI-DTP screening data was reported,[12] together with case studies of potent antiproliferative imidazolium derivatives[13] and histone deacetylase inhibitors.[14]

Continuing our interest in glutarimide derivatives,[15] a structure–activity study is reported herein on the antiproliferative activity of a set of glutarimide-containing compounds (**1**–**22**) toward K562 (leukaemia), A549ATCC (non-small cell lung), malme-3M (melanoma), COLO205 (colon), UO31 (renal), U251 (CNS), IGROV1 (ovarian), and MFC-7 (breast) human tumour cell lines; which are described in the text as models **A**–**H**, respectively. Data were taken from the US National Cancer Institute (NCI) Developmental Therapeutics Program 60 human tumours cell line screen database (NCI60).[16] The results obtained in this study could be a guidance for the design of novel congeners with expected antiproliferative activity. To the best of our knowledge, structure–activity relationships of the antiproliferative potency of glutarimide derivatives cannot be found in the literature.

RESULTS AND DISCUSSION

Aimed at finding the pharmacophoric pattern of glutarimide derivatives responsible for their significant antiproliferative activity, alignment-independent 3D QSAR models for the potency of **1**–**22** toward representative cell lines were obtained. The criteria for the selection of the compounds are given in the Experimental. Within each category, the cell line towards which most of the glutarimide derivatives exert activity were chosen. The structures and classification of the compounds are given in Table I.

Methodology

The program Pentacle[17] uses alignment independent descriptors derived from GRID[18] molecular interaction fields (MIF). A more negative value of GRID MIF for any used probe corresponds to a more favourable interaction between the

TABLE I. Structures of **1**–**22** used in the models

Class No.[a]	Structure	Compound No.
I	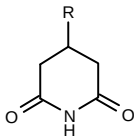 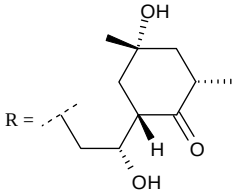	**1**
	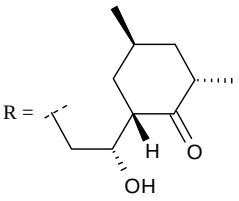	**2**
	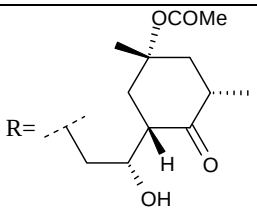	**3**
II	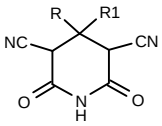 R = Me– R_1 = 2-Cl–Ph–	**4**
	R = Me– R_1 = 4-F–Ph–	**5**
III	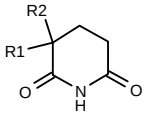 R_1 = *n*-hept– R_2 = 4-NH_2–Ph–	**6**

TABLE I. Continued

Class No.[a]	Structure	Compound No.
IV	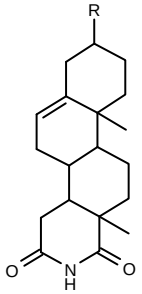 R = –OC(O)Me	**7**
	R = –OH	**8**
V	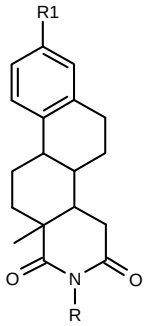 R = $–CH_2CH_2–$Pyr R_1 = –O–Me	**9**
	R = H– R_1 = –O–Me	**10**
	R = Me– R_1 = –O–Me	**11**
	R = *n*-Bu– R_1 = –O–*n*-Bu	**12**
	R = *n*-Bu– R_1 = $–O–CH_2CH_2–$Pyr	**13**
	R= -O-$CH_2CH_2–$Pip R_1= –O–Me	**14**
	R = $–NH_2$ R_1 = –O–Me	**15**
VI	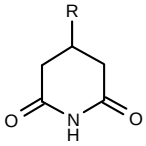 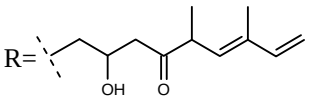	**16**
	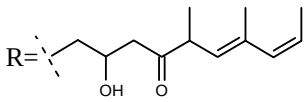	**17**
VII	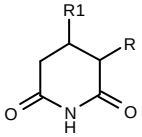 R = –C(O)O–*t*-Bu 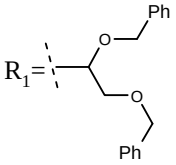	**18**
VIII	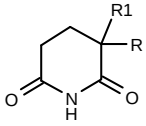 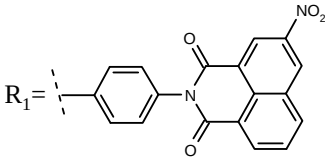	**19**
	R = Et–	

TABLE I. Continued

Class No.[a]	Structure	Compound No.
IX	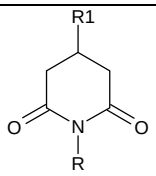 R = Ph– 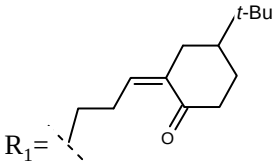 R_1=	**20**
	R= Ph– 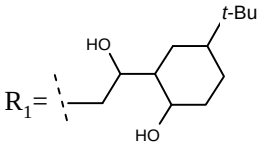 R_1=	**21**
X	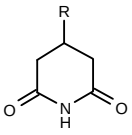 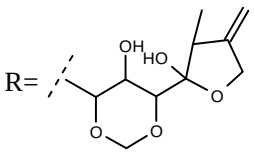	**22**

probe (*e.g.*, hydrogen bond donor, hydrogen bond acceptor, hydrophobic) and a molecule for which the GRID MIF was calculated. By calculating MIFs for different GRID probes around the molecule and extracting the most relevant regions, a fingerprint of a receptor to which a small molecule could fit well can be obtained. These regions show favourable energy of interaction and represent positions where groups of a potential receptor would interact favourably with a ligand. Such an MIF pattern can be described as the virtual receptor site (VRS). Each GRIND descriptor consists of two nodes extracted from MIFs and encodes their energy product and spatial distance. GRIND variables represent geometrical relationships between relevant pharmacophore points around the studied molecules, which are invariable with respect to the position of the molecule in space and their alignment. The derivation of GRIND descriptors includes the following steps: *i*) computing a set of MIF around the studied molecules, *ii*) filtering the MIF, to extract the most relevant regions that define the VRS and *iii*) encoding the VRS into the GRIND variables. GRIND variables can be used for comparison of molecules and their classification within sets of structurally diverse entities and the Pentacle program uses principal component analysis (PCA) for this type of analysis. A dependent variable (*e.g.*, biological activity) can be correlated to GRIND descriptors (as independent variables) obtained on a set of molecules by partial least square analysis (PLS). The most intensive bars in the PLS plots have the highest impact on the model. Bars having positive values on the *y* scale represent variables positively correlated with activity, while those having nega-

tive values on *y* scale are negatively correlated with activity. Within each block (auto or cross-correlograms, which correspond to pairs of nodes of the same or a different probe, respectively) variables are arranged from left to right on the *x* scale of the plot according to ascending distance between their nodes. In addition to the spatial arrangement of molecules and nodes encoded in the GRIND variables, each node of each variable exerts a specific energy of interaction with a target molecule. Therefore, the strength of the interaction between a respective GRID probe in a particular node and the molecules are presented as well as the spatial positions of the VRS regions.

The NCI60 anticancer drug screen[16] was developed in the late 1980s, and was quickly recognized as a rich source of information concerning the mechanisms of growth inhibition and tumour-cell kill. Recently, its role has evolved to that of a service screen supporting the cancer research community.

Structure–activity relationship

The potencies of compounds, given as p(GI_{50}), the negative logarithm of the molar concentration that induces a 50 % reduction of the respective cell growth, are given in Table I-S in the Supplementary material. Eight models were built. All the studied compounds (**1**–**22**) exhibited a similar order of potency towards each cell line, as can be seen from Table I-S, and the intercorrelation matrix of the p(GI_{50}) values for all the studied cell lines (Table XV-S). As all the obtained models were similar in their important parts, a detailed description of the model on the antiproliferative potency of **1**–**22** towards the K562 cell line is given and explained. For the other cell lines, the partial least square coefficient plots, statistical data, and the expression of variables for each compound are given in the supplementary material in tabular format.

The variables of the models positively or negatively correlated with activity readily detected the structural motifs of compounds **1**–**22** that contribute to potency. The smaller molecules were more potent towards all the studied cell lines. Molecules containing both the glutarimide moiety and a HBA, mainly the hydroxyl group, on a spatial distance of ~11 Å expressed higher potency. On the contrary, larger molecules and those with bulky substituents at a distance of ~20 Å from the glutarimide moiety were significantly less potent. The characteristic PLS plot obtained with 4 latent variables (LV) for the K562 model is given in Fig. 1d.

– All the described structural motifs of the compounds important for the antiproliferative potency are anchored to the glutarimide moiety that comprises HBA, HBD, and hydrophobic parts.

– Two hydrophobic moieties, one of which is associated with alkyl part of the glutarimide ring and the other with the distal (8.32–8.64 Å) π systems of the molecules, are negatively correlated with the potency of the compounds – vari-

able DRY–DRY 26 (Fig 1a). Accordingly, this variable is not expressed for the most potent **22**.

– Compounds that comprise two HBD groups at a distance of ~11 Å exert higher potencies. One HBD is always glutarimide, –NH–, while the other is hydroxyl group, positioned at the topological distance of five bonds for **22**, or at the methylene bridge for **1**–**3** (Table I), as given by the variable O–O 111, Fig. 1b.

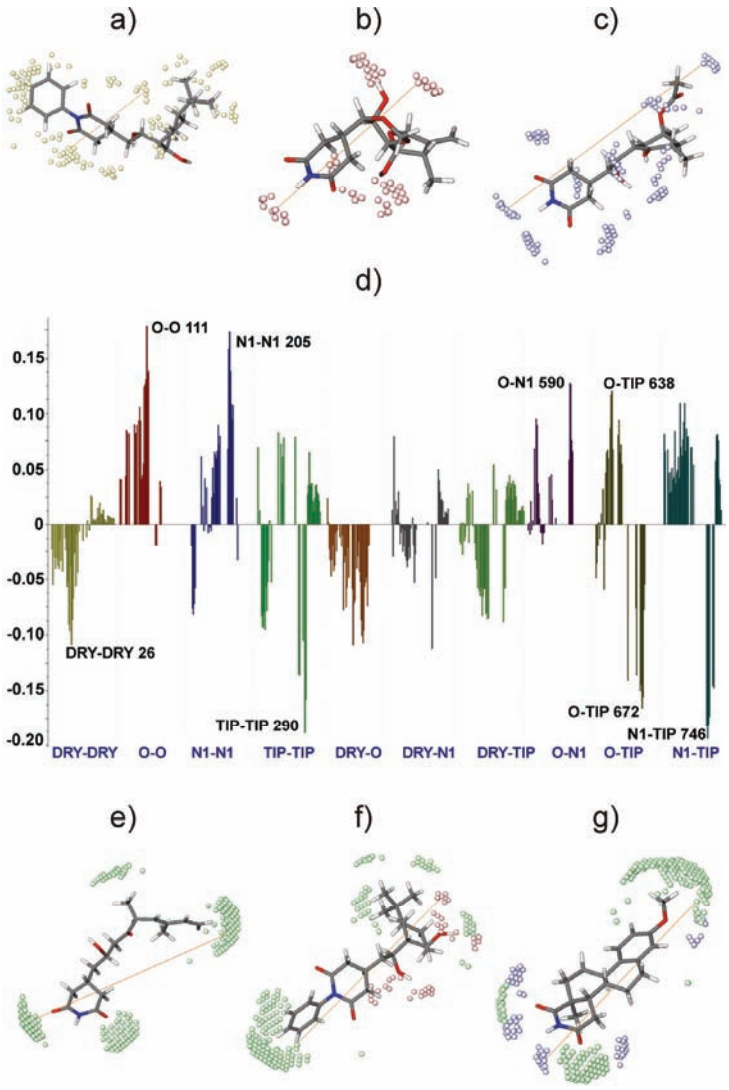

Fig. 1. Examples of variables that have a high impact on the model, associated with compounds: a) variable DRY–DRY 26 for **21**; b) variable O–O 111 for **22**; c) variable N1–N1 205 for **3**; d) 4 LV PLS coefficient plot for the K562 model; e) variable TIP–TIP 290 for **16**; f) variable O–TIP 672 for **21**; g) variable N1–TIP 746 for **10**.

– Two HBA groups at a distance of ~16.8 Å are the next structural motif positively correlated with activity, as given by variable N1–N1 205, Fig. 1c. This variable exists only for compounds of class V and compounds **1** and **3**, which belong to the most potent class I. For compounds of class V, one HBA is always glutarimide >C=O and the other is an alkoxy group, except for compound **13**, which is more potent than the other members of this class. In this point, the model recognized the HBA of the pyrrolidino substituent in place of the alkoxy group of the other compounds within class V. In **1** and **3** (class I), the other HBA is the distal –OH or the carbonyl oxygen of the methyl ester, respectively.

– All structural motifs, as described above, that have a significant impact on the models emphasize that all highly potent molecules bear similar spatially positioned HBD–HBD and HBA–HBA combinations, as exemplified in Figs. 1b and 1c.

– The bulkier compounds exhibited a lower potency ($p(GI_{50}) < 6$), as can be seen from the variable TIP–TIP 290, Fig. 1e. The glutarimide ring distal from bulky substituents, *i.e.*, a terminal methyl or *t*-butyl group; or the glutarimidonaphthyl moiety (classes VI, VIII and IX, respectively), negatively influences the potency. Molecules of the most potent classes (I and X) and some less potent molecules from classes III and IV lack bulky substituents distal from the glutarimide moiety.

– Similar information encoded in variables that have the highest positive impact on the model (O–O 111, N1–N1 205) could be obtained from the additional variables O–N1 590 and O–TIP 638, respectively. Therefore, HBA and HBD of molecules positioned at a spatial distance of ~16.8 Å significantly contribute to the potency. The variable O–N1 590 is expressed for the potent **1** and **3** (class I), as well as for **10** and **15** (class V), see Table VII-S. Implicitly, compounds from class V that have similarly positioned HBA and HBD as in compounds of class I but a rigid backbone exhibit lower potencies. Together with this, structural motifs comprising HBD at ~7.2 Å from the non-polar part of the molecules contribute to the potency.

– Variables O–TIP 672 and N1–TIP 746 offer similar information as the variable TIP–TIP 290. Those variables show that compounds having bulky substituents (TIP) distal from the glutarimide moiety (O or N1) have lower potency.

The structural differences between the most and the least potent compounds can be clearly seen from Pentacle heatmaps (see the experimental for an explanation of matrix representation of correlograms). The heatmaps for the whole set (**1**–**22**) are presented in Fig. 2. The compounds are arranged by decreasing potencies, from top to bottom. A distinct band of O–O correlograms exists for the most potent compounds (yellow framed), which is consistent with the significance of the O–O variables that have a strong positive impact on the model. For the other compounds, the regions of the same correlograms are less populated.

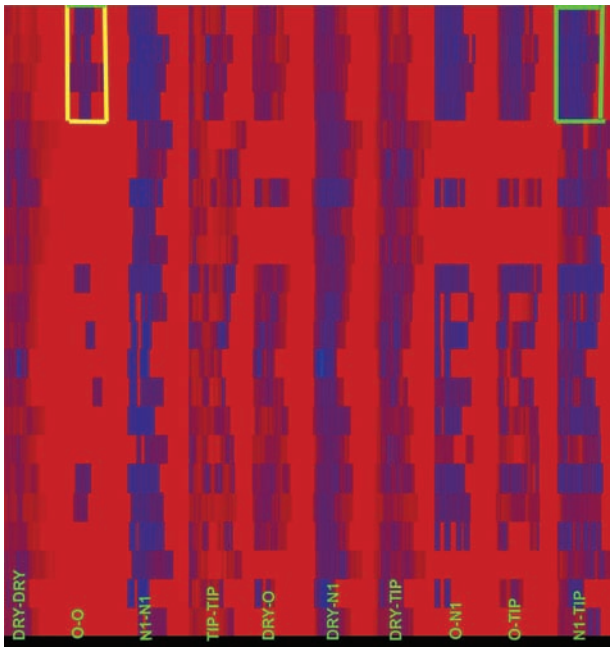

Fig. 2. Matrix-like representation (heatmaps) of the auto- and cross-correlograms of **1**–**22**.

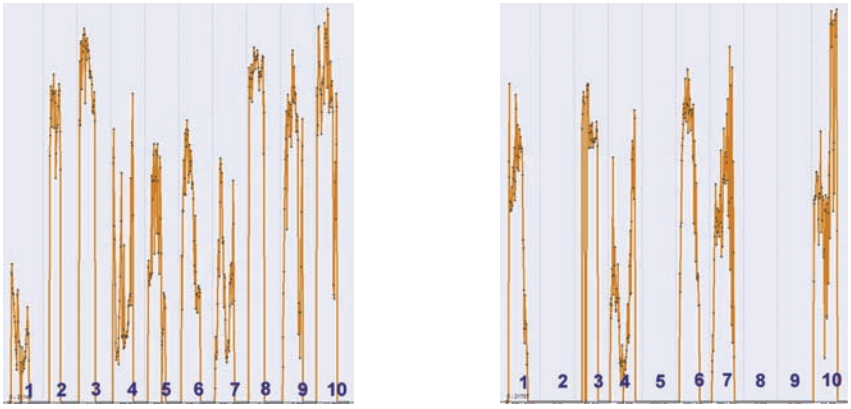

(a) (b)

Fig. 3. Auto- and cross-correlograms of compounds a) **22** and b) **11**, labelled as follows: **1** DRY–DRY, **2** O–O, **3** N1–N1, **4** TIP–TIP, **5** DRY–O, **6** DRY–N1, **7** DRY–TIP, **8** O–N1, **9** O–TIP and **10** N1–TIP.

Together with this, the bands of the TIP–TIP correlograms are broader for the larger, less potent compounds; while the band of the N1–TIP block is narrower for the most potent compounds (framed green), which is consistent with the description of the N1–TIP variables that describe larger node–node distances, and has a high negative impact on potency in all models. As an additional illustration,

all auto- and cross-correlograms for the most (**22**), and one of the least potent (**11**) compounds are given in Figs. 3a and 3b, respectively. Comparing the most important differences in the pattern of the most **22** and less potent **11**, it is evident that the less active compound lacks two HBD (empty O–O block (2)) and the larger strong peaks in the TIP–TIP block (4) are positioned to the right with respect to the same block of **22.** Additionally, there is significantly larger distance between one HBA and the distal part of molecule in the less potent **11** than in **22**, as shown by the strong peaks in the N1–TIP block (10), positioned to the right for **11** compared to **22**.

To summarize the observations mentioned above, two plots are presented in Fig. 4 in which the potency of the compounds (p(GI_{50})) is plotted *vs*. the molecular volume and *vs*. the distance between the glutarimide moiety and the distal HBA or HBD. A clear separation of the most potent compounds was achieved in this way.

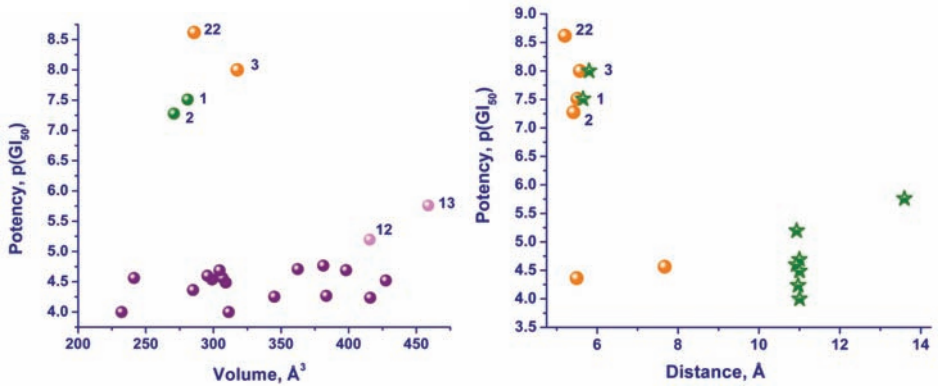

(a) (b)

Fig. 4. a) p(GI_{50}) *vs*. volume of **1**–**22**. The compounds are coloured according to their increasing potencies, in the following order: purple–pink–green–orange. b) p(GI_{50}) *vs*. HBA/HBD distance, given as: HBD–HBD of the compounds associated to the variable O–O 111 (orange spheres) and HBA–HBA of the compounds associated to the variable N1–N1 205 (green stars).

EXPERIMENTAL

The NCI-DTP Database was searched for structures comprising the glutarimide moiety (substructure query as SMILES notation: O=C1CCCC(=O)N1). All compounds that matched the query were saved (**1**–**22**) and their potency expressed as p(GI_{50}) against: leukaemia K562 (**A**); non small cell lung A549ATCC (**B**); colon COLO205 (**C**); CNS U251 (**D**); melanoma malme-3M (**E**); ovarian IGROV1 (**F**); renal UO-31 (**G**) and breast MCF-7 (**H**) tumour cell lines extracted. SMILES Notation of **1**–**22** was converted to 3D by CORINA.[19] Each initial 3D structure was imported in VegaZZ[20] and twenty conformations that represent local minima were obtained by conformational search on the MM level (MMFF94s force field),[21] using the Boltzmann jump algorithm in AMMP.[22] Each conformation of each compound was mini-

mized by the semi-empirical molecular orbital PM6 method,[23] using implicit solvation in water (COSMO) to root mean square gradient of 0.01; by MOPAC2009.[24] The obtained conformation of each compound that had the lowest heat of formation (implied the most stable one) were chosen for model building. All molecules were treated in their neutral form.

For alignment-free 3D QSAR analysis, the molecules were submitted to Pentacle.[17] The molecular interaction fields were computed using the built-in GRID program,[18] with a grid resolution of 0.4 Å. AMANDA algorithms were used for the extraction of hot spots (nodes) from the obtained MIFs (discretization); the distances and relative position of the nodes were described by maximum auto and cross-correlation (MACC2) (encoding). For details, see the original reference.[17] Five principal components/latent variables were used for the initial principal component analysis (PCA) and partial least square (PLS) model. Selection of the variables was realised by one cycle of factorial fractional design (FFD) for the models **A**–**H**. Validation of the models was performed by cross validation using four groups of approximately the same size in which the objects are assigned randomly. The final models were obtained with 3 or 4 latent variables (LV).

A detailed explanation of auto- and cross-correlogram in the ALMOND program can be found in the original reference[25] and the program manual available from the Molecular Discovery web site. Exactly the same correlograms can be found in Pentacle, with the option of a matrix-like presentation of the auto- and cross-correlograms for all compounds, named heatmaps, as depicted in Fig. 2. In the matrix-like representation, every row represents a single compound and every column a single variable. The values of the variables are colour-coded from red (low value) to blue (high value).

Details of the procedure for the determination of GI_{50} values can be found at: http://dtp.nci.nih.gov/branches/btb/ivclsp.html and in the literature.[26]

CONCLUSIONS

It can be concluded that, generally, smaller molecules are more potent towards all studied cell lines. Molecules containing the glutarimide moiety at a distance ~11 Å, or 5 topological bonds, to a HBA (mainly hydroxyl group) express higher potencies. On the contrary, larger molecules and those with bulky substituents at a distance ~20 Å from the glutarimide moiety are significantly less potent. In addition, it was noticed that within a subset having a favourable pharmacophore pattern, as described above, molecules possessing a flexible backbone (classes I and X) are more potent than rigid tetracyclic molecules (class V). These conclusions will be guidance for the selection of compounds previously prepared for *in vitro* antitumour screening; as well as for the design and syntheses of novel compounds that could express significant potency towards dedifferentiated human cells.

SUPPLEMENTARY MATERIAL

Associated with this article; p(GI_{50}) values for **1**–**22** towards cell lines **A**–**H**, PCA models, PLS models, PLS plots, structural motifs associated with important variable for the cell line models **A**–**H**, association of variables with **1**–**22** for cell line models **A**–**H** and the intercorrelation matrix of p(GI_{50}) values for all the reported cell lines are available electronically from http://www.shd.org.rs/JSCS/, or from the corresponding author on request.

Acknowledgements. The corresponding author gratefully acknowledges Professor Milovan D. Ivanović for moral support and great interest in the modelling study. This work was supported by the Ministry of Science and Technological Development of the Republic of Serbia (Project Nos. 142074 and 142010).

И З В О Д

АНТИПРОЛИФЕРАТИВНА АКТИВНОСТ ГЛУТАРИМИДНИХ ДЕРИВАТА ИЗ БАЗЕ ПОДАТАКА НАЦИОНАЛНОГ ИНСТИТУТА ЗА РАК, САД. 3Д ОДНОС СТРУКТУРЕ И АКТИВНОСТИ НЕЗАВИСАН ОД ПОРАВНАВАЊА МОЛЕКУЛА

ЈЕЛЕНА Б. ПОПОВИЋ-ЂОРЂЕВИЋ[1], ЉИЉАНА И. ДОШЕН-МИЋОВИЋ[2], ИВАН О. ЈУРАНИЋ[2] и БРАНКО Ј. ДРАКУЛИЋ[3]

[1]Пољопривредни факултет , Универзитет у Београду, Немањина 6, 11080 Београд, [2]Хемијски факултет, Универзитет у Београду, Студентски трг 12–16, 11000 Београд и [3]Институт за хемију, технологију и металургију – Центар за хемију, Универзитет у Београду, Његошева 12, 11000 Београд

У тексту је описан однос структуре и антипролиферативне активности 22 глутаримидна деривата према осам репрезентативних линија хуманих тумора. Подаци о структури једињења и њиховој активности су преузети из базе података Националног Института за рак, САД. Дескриптори, независни од поравнавања молекула (GRIND-2), коришћени у проучавању односа структуре и активности су добијени употребом програма GRID. Модели јасно приказују структурне елементе једињења који се позитивно или негативно корелишу са биолошком активношћу. Фармакофорна слика добијена из модела ће бити коришћена за планирање нових аналога који садрже глутаримидни прстен и за које се очекује да ће показати значајну антипролиферативну активност.

(Примљено 2. децембра 2009, ревидирано 25. јануара 2010)

REFERENCES

1. a) M. E. Salvati, A. Balog, W. Shan, D. D. Wei, D. Pickering, R. M. Attar, J. Geng, C. A. Rizzo, M. M. Gottardis, R. Weinmann, S. R. Krystek, J. Sack, Y. An, K. Kish, *Bioorg. Med. Chem. Lett.* **15** (2005) 271; b) A. L. Machado, L. M. Lima, J. X. Araújo Jr., C. A. M. Fraga, V. L. G. Koatz , E. J. Barreiro, *Bioorg. Med. Chem. Lett.* **15**, (2005) 1169; c) J. Kossakowski, M. Jarocka, *Farmaco* **56** (2001) 785; d) J. J. Wang, S. S. Wang, C. F. Lee, M. A. Chung, Y. T. Chern, *Chemotherapy* **43** (1997) 182; e) H. Miyachi, A. Azuma, A. Ogasawara, E. Uchimura, N. Watanabe, Y. Kobayashi, F. Kato, M. Kato, H. Hashimoto, *J. Med. Chem.* **40** (1997) 2858
2. a) F. Matsuda, S. Terashima, *Tetrahedron* **44** (1988) 4721; b) R. G. Powel, C. R. Smith, D. Weisleder G. K. Matsumoto, J. Clardy, J. Kozlovsky, *J. Am. Chem. Soc*. **105** (1983) 3739
3. M. I. Andres, P. Sanz, A. Garfia, G. Repetto, M. Repetto, *In Vitro Mol. Toxicol.* **10** (1997) 319
4. D. K. K. Ha, W. H. Lau, *Cancer Lett.* **41** (1988) 217
5. Y. Ishikawa, M. Tachibana, C. Matsui, R. Obata, K. Umezawa, S. Nishiyama, *Bioorg. Med. Chem. Lett.* **19** (2009) 1726
6. J. Newell-Price, *Cushing's disease*, in *Clinical Endocrine Oncology*, 2nd ed., I. D. Hay, J. A. H. Wass, Eds., Blackwell Publishing, Malden, MA, 2008, p. 253
7. 7. P. E. Lanning, D.C. Jahannessen, *Drugs Today* **27** (1991) 117

8. 8. R. J. Santen, H. Brodie, E. R. Simpson, P. K. Siiteri, A. Brodie, *Endocr. Rev.* **30** (2009) 343
9. D. S. Fischer, L. W. L. Woo, M. F. Mahon, A. Purohit, M. J. Reed, B. V. L. Pottera, *Bioorg. Med. Chem.* **11** (2003) 1685
10. R. J. Snow, M. G. Cardozo, T. M. Morwick, C.A. Busacca, Y. Dong, R. J. Eckner, S. Jacober, S. Jakes, S. Kapadia, S. Lukas, M. Panzenbeck, G. W. Peet, J. D. Peterson, A. S. Prokopowicz, R. Sellati, R. M. Tolbert, M. A. Tschantz, N. Moss, *J. Med. Chem.* **45** (2002) 3394
11. a) M. Pastor, in: *Methods and Principles in Medicinal Chemistry*, *Molecular Interaction Fields: Applications in Drug Discovery and ADME Prediction*, G. Cruciani, Ed., Wiley--VCH, Weinheim, 2006, p. 117; b) A. Duran, I. Zamora, M. Pastor, *J. Chem. Inf. Model*. **49** (2009) 2129
12. G. Cruciani, P. Benedetti, G. Caltabiano, D. F. Condorelli, C. G. Fortuna, G. Musumarra, *Eur. J. Med. Chem.* **39** (2004) 281
13. a) F. P. Ballistreri, V. Barresi, P. Benedetti, G. Caltabiano, C. G. Fortuna, M. L. Longoa, G. Musumarra, *Bioorg. Med. Chem*. **12** (2004) 1689; b) C. G. Fortuna, V. Barresi, G. Berellini, G. Musumarra, *Bioorg. Med. Chem*. **16** (2008) 4150
14. R. Ragno, S. Simeoni, D. Rotili, A. Caroli, G. Botta, G. Brosch, S. Massa, A. Mai, *Eur. J. Med. Chem*. **43** (2008) 621
15. J. B. Popović-Djordjević, M. D. Ivanović, V. D. Kiricojević, *Tetrahedron Lett.* **46** (2005) 2611
16. R. H. Shoemaker, *Nat. Rev. Cancer* **6** (2006) 813
17. Á. Durán, G. C. Martínez, M. Pastor, *J. Chem. Inf. Model.* **48** (2008) 1813; Pentacle 1.0.3, http://cadd.imim.es/grib-cadd/projects/pentacle or http://www.moldiscovery.com (accessed on 29/09/2009)
18. P. J. Goodford, *J. Med. Chem.* **28** (1985) 849; GRID22b, http://www.moldiscovery.com (accessed on 29/09/2009)
19. a) J. Sadowski, J. Gasteiger, *Chem. Rev*. **93** (1993) 2567; b) J. Sadowski, J. Gasteiger, G. Klebe, *J. Chem. Inf. Comput. Sci*. **34** (1994) 1000
20. A. Pedretti, L. Villa, G. Vistoli, *J. Comput.-Aided Mol. Des.* **18** (2004) 167; VegaZZ 2.0.3, http://www.ddl.unimi.it/ (accessed on 29/09/2009)
21. T. A. Halgren, *J. Comput. Chem.* **20** (1999) 720
22. R. W. Harrison, *J. Comput. Chem.* **14** (1993) 1112
23. J. J. P. Stewart, *J. Mol. Model.* **13** (2007) 1173
24. J. J. P. Stewart, *J. Comput.-Aided Mol. Des.* 4 (1990) 1; J. J. P Stewart, *MOPAC2009*, Stewart Computational Chemistry, Colorado Springs, CO, 2009, http://OpenMOPAC.net (accessed on 29/09/2009)
25. M. Pastor, G. Cruciani, I. McLay, S. Pickett, S. Clementi, *J. Med. Chem.* **43** (2000) 3233
26. M. C. Alley, D. A. Scudiero, P. A. Monks, M. L. Hursey, M. J. Czerwinski, D. L. Fine, B. J. Abbott, J. G. Mayo, R. H. Shoemaker, M. R. Boyd, *Cancer Res.* **48** (1988) 589; http://dtp.nci.nih.gov/branches/btb/ivclsp.html (accessed on 29/09/2009).